ELSEVIER

Catalysis Today 66 (2001) 97–103

CATALYSIS TODAY

www.elsevier.com/locate/cattod

Anisotropic ordering of Mo species deposited on TiO_2(1 1 0) characterized by polarization-dependent total reflection fluorescence EXAFS (PTRF-EXAFS)

Wang-Jae Chun [a,1], Kiyotaka Asakura [b,*], Yasuhiro Iwasawa [a]

[a] *Department of Chemistry, Graduate School of Science, The University of Tokyo, 7-3-1 Hongo, Bunkyo-ku, Tokyo 113-0033, Japan*
[b] *Catalysis Research Center, Hokkaido University, Sapporo 060-0811, Japan*

Abstract

Structure of Mo species deposited on a TiO_2(1 1 0) surface has been studied using in situ polarization-dependent total reflection fluorescence EXAFS (PTRF-EXAFS). We found anisotropic ordering of the Mo species reflecting the anisotropic structure of TiO_2 surface when $Mo(CO)_6$ was deposited under reductive conditions. Mo chains were produced with its Mo–Mo bonding parallel to the [0 0 1] direction of the TiO_2 substrate. The results provide a possible way to regulate the structure of Mo species on TiO_2(1 1 0) by the preparation conditions.

Keywords: Polarization-dependent total reflection fluorescence EXAFS (PTRF-EXAFS); Chemical vapor deposition (CVD); TiO_2(1 1 0); $Mo(CO)_6$; Mo chain growth

1. Introduction

Active metal site–support interface interaction is one of the key issues to understand the properties of supported catalysts. Numerous studies have been carried out on the support effects on the catalyses but there are a limited number of reports on the interface structures on atomic levels. One approach to this problem is to investigate metal growth on well-defined single crystal oxide surfaces. TiO_2(1 1 0) is one of the most widely studied metal oxide surfaces thus far [1–6]. The TiO_2(1 1 0) surface has an anisotropic structure with oxygen rows running parallel to the [0 0 1] direction as shown in Fig. 1a. Between the bridging oxygen rows, there is a channel composed of fivefold Ti along the [0 0 1] direction. The structure of deposited metal species may be affected by the specific surface structure of TiO_2(1 1 0) [4,7–22]. Xu et al. reported that Pd dimers grow parallel to the [0 0 1] direction of TiO_2(1 1 0). Onishi et al. [13] measured angle resolved XPS of Ni/TiO_2 and claimed that Ni–Ni bond was arranged on the Ti channel in the [0 0 1] direction. Many other deposited metals have been reported to have metal–metal bond along the [0 0 1] axis of TiO_2(1 1 0) surface [9–11,14,18–21]. Thus the overlayer structures seem to preferentially align with the [0 0 1] direction, i.e., parallel to the bridging oxygen.

On the other hand, we have investigated Mo oxides on a TiO_2(1 1 0) surface using the polarization-dependent total reflection fluorescence extended X-ray absorption fine structure (PTRF-EXAFS) technique [16,17]. We found that anisotropic Mo dimers were selectively formed on the TiO_2(1 1 0) surface, with the Mo–Mo bond direction perpendicular to the oxygen rows [16,17]. The bond direction of Mo–Mo is different from those of the other deposited metals.

* Corresponding author.
[1] Present address: CAC, Inc., Tsukuba Laboratory, 8-3-1 Chu-o, Ami, Inashiki, Ibaraki 300-0332, Japan.

0920-5861/01/$ – see front matter
PII: S0920-5861(00)00609-X

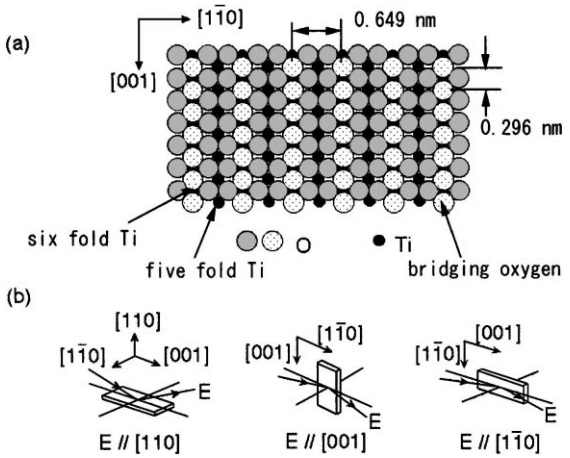

Fig. 1. (a) Surface structure of TiO_2(1 1 0) and (b) schematic illustration of 3-direction measurements.

The difference in metal–metal bond direction can be attributed to the difference in oxidation state. In the former case where metal–metal alignment is parallel to the [0 0 1] direction, the overlayer metal species are in a metallic state, while Mo species in the latter case are situated in 6+ oxidation state. In this paper we prepared low-valent Mo species on TiO_2(1 1 0) by chemical vapor deposition (CVD) of $Mo(CO)_6$ as a precursor under reductive conditions in order to regulate the metal arrangement on the above hypothesis. The deposited Mo species was characterized by means of PTRF-EXAFS.

The PTRF-EXAFS is a promising technique to determine the orientation, location and three-dimensional interface structure of the deposited metal species even without a long-range order [16,17,22,23]. It can determine bond distances with the accuracy of at least 0.01 nm. The principle of the PTRF-EXAFS is based on polarization-dependence of EXAFS oscillation $\chi(k)$ as shown in Eq. (1).

$$\chi(k) = \sum_i 3\cos^2\theta_i \, \chi_i(k) \quad (1)$$

where θ_i is an angle between the ith bond direction and the electric vector of incident X-rays, and $\chi_i(k)$ is a partial EXAFS oscillation accompanying the ith bond. Thus the coordination number derived from polarization-dependent EXAFS (called as effective coordination number) is three times as large as the real one when the bond direction is parallel to the electric vector but the effective coordination number is zero when the bonding is perpendicular to the electric vector. Since conventional supported catalysts are in a powder form, Eq. (1) is averaged over all directions and the obtained structural information is a merely averaged one. However, when one employs a single crystal surface as a model support where the bond direction is fixed to a laboratory coordinate, one can get polarization-dependent EXAFS of metal species dispersed on it as expressed by Eq. (1). The problem is the small amount of surface deposited species on a small surface area of single crystal, i.e., 10^{14}–10^{15} atoms cm^{-2}. One can solve this problem by using a fluorescence detection method. In addition the total reflection measurement can increase surface sensitivity and decrease scattering X-rays from the bulk [24,25].

2. Experimental

2.1. Sample preparation

A polished TiO_2(1 1 0) single crystal ($20 \times 40 \times 1\,mm^3$) (Earth Jewelry) with an optical grade was washed several times with ultra pure water (18 mΩ; Millipore) and then calcined at 823 K for 2 h in air. Chemical vapor deposition of $Mo(CO)_6$ was performed in a quartz cell in a closed system. The cell was composed of two compartments separated by a grease-free valve which was closed first. The whole cell was covered completely with Al-foil to prevent photodecomposition of $Mo(CO)_6$. One compartment contains $Mo(CO)_6$ powder in a high purity Ar and the pretreated single crystal was put in the other compartment of the cell which was evacuated for 2 h. After the grease-free valve was opened and the Ar was removed for 5 min, the cell was filled with 100 Torr H_2 and the single crystal was interacted with $Mo(CO)_6$ at 363 K for 6 h. Molybdenum loading was determined by XPS and estimated to be 0.2 ML (1 Mo atom nm^{-2}).

2.2. PTRF-EXAFS measurement

PTRF-EXAFS spectra were measured at BL14A vertical wiggler beam line of the photon factory in the Institute of Material Structure Science in High

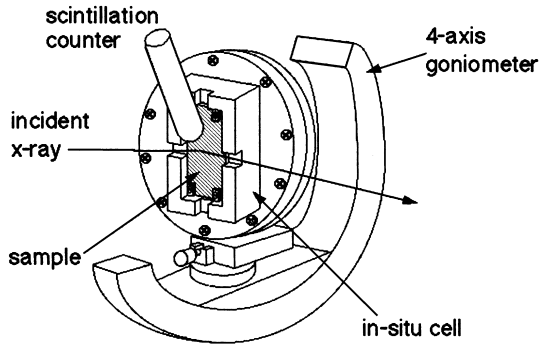

Fig. 2. In situ PTRF-EXAFS cell.

Energy Accelerator Research Organization (KEK-PF). The synchrotron radiation was monochromatized by a Si (3 1 1) double-crystal monochromator. The storage ring was operated at 2.5 GeV with 200–350 mA. Mo K-edge EXAFS spectra were recorded in the range from 19 780 to 20 500 eV with an energy interval of 3 eV at room temperature. The X-ray beam size was reduced to 0.1 mm ϕ in diameter by a pin-hole in order to avoid unnecessary irradiation around the sample. Incident and reflected X-rays were monitored by 50 and 270 mm long ionization chambers filled with Ar, respectively. Fluorescence X-rays coming from the sample were detected by a small-head NaI(Tl) scintillation counter (14 mm ϕ). Since the TiO_2(1 1 0) surface has an anisotropic structure as shown in Fig. 1a, PTRF-EXAFS measurements were carried out in three different directions against the electric vector of the incident X-rays, i.e., the [1 $\bar{1}$ 0], [0 0 1] and [1 1 0] directions of TiO_2(1 1 0) as shown in Fig. 1b. The sample was transferred to an in situ PTRF-EXAFS cell as shown in Fig. 2 in a high purity N_2-filled glove box without exposure to air. The Al-made cell has five windows sealed with Kapton (thickness: 200 μm) for preventing exposure of the sample to air. The sample chamber was mounted on a high precision four-circle goniometer [16,17].

2.3. Data analysis

Absorbance, μt, was calculated directly from the intensity ratio of the fluorescence X-ray detected by a scintillation counter (I_f) to the incident X-ray signal detected by an ionization chamber (I_0) without any correction such as self-absorption because absorbers are all on the surface. The EXAFS oscillation, $\chi(k)$, was extracted from the μt by a spline smoothing method and was normalized by the edge height using the EXAFS analysis program REX ver. 2.5 coded by Rigaku [26]. The energy dependence of the edge height was taken into account using the McMaster equation. The origin of kinetic energy of photoelectron was taken to be an inflection point of the edge jump.

3. Results

Fig. 3 shows Mo K-edge PTRF-XANES (X-ray absorption near edge structure) spectra with three different directions. A characteristic peak assigned to 1s → 4d was observed in the spectra parallel to the [1 $\bar{1}$ 0] and [1 1 0] directions, while the spectrum parallel to the [0 0 1] direction of TiO_2(1 1 0) did not show such a pre-edge peak. The peak position was about 20 000 eV. It implies an asymmetric growth of the Mo species on TiO_2(1 1 0). Such a pre-edge

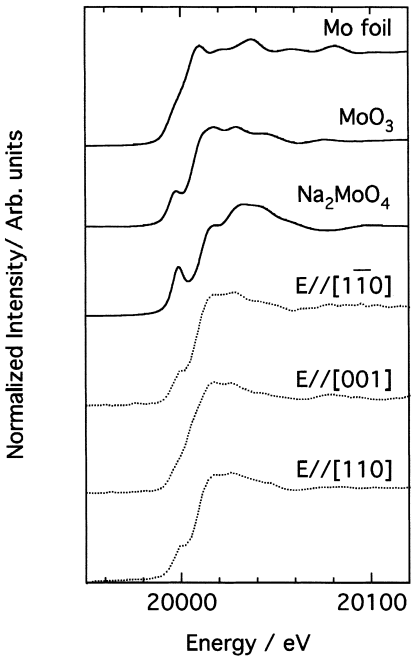

Fig. 3. Normalized PTRF-XANES spectra for Mo/TiO_2(1 1 0) and reference samples.

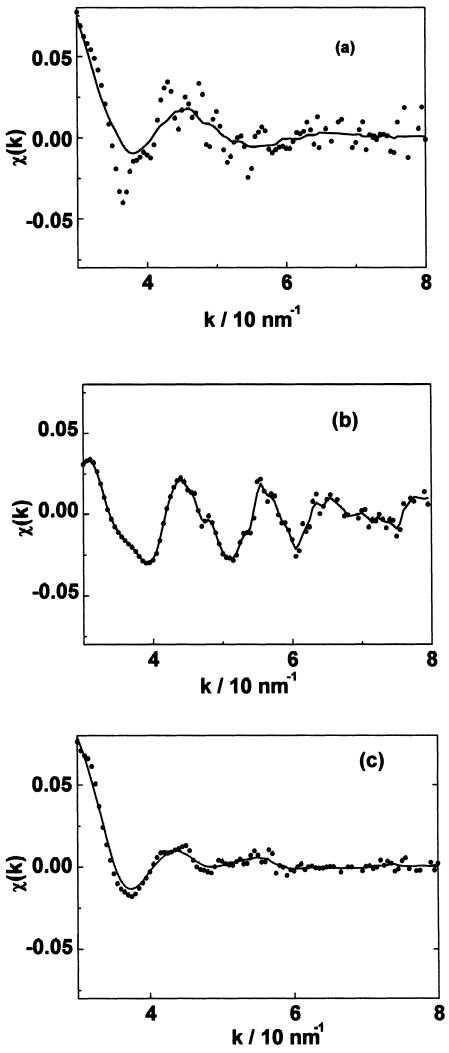

Fig. 4. Background subtracted raw PTRF-EXAFS oscillations: (a) $\vec{E}//[1\,\bar{1}\,0]$, (b) $\vec{E}//[0\,0\,1]$ and (c) $\vec{E}//[1\,1\,0]$, where $\vec{E}$ is the electric vector of the incident X-ray.

peak is often related to the direction of double bond oxygen [27]. Thus the Mo–O bond may be present in these two directions.

Fig. 4 shows Mo K-edge PTRF-EXAFS oscillations for the $[1\,\bar{1}\,0]$, $[0\,0\,1]$ and $[1\,1\,0]$ orientations of $TiO_2(1\,1\,0)$. Different oscillations for each direction indicate again that Mo species on $TiO_2(1\,1\,0)$ has an anisotropic surface structure. A clear oscillation appeared in the $[0\,0\,1]$ direction, while the EXAFS oscillations in the other directions damped quickly. The

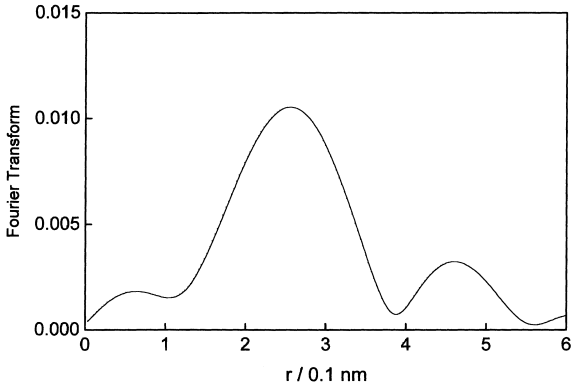

Fig. 5. Fourier transform of the PTRF-EXAFS oscillation of $\vec{E}//[0\,0\,1]$ in the range of $k = 30$–$80\,\mathrm{nm}^{-1}$.

k-dependence of EXAFS amplitude is mainly determined by the type of scatterer. Light scatterers like O and C show a monotonous reduction in EXAFS oscillation amplitude, though the backscattering amplitude took maximum at high *k*-region for heavy scatterers like Mo [30]. Thus the *k*-dependence of EXAFS amplitude in the three different directions indicates that the Mo–Mo bond is present only in the $[0\,0\,1]$ direction. This is contrasted to the structure of Mo^{6+}/TiO_2 prepared under oxidative conditions which has the Mo–Mo direction perpendicular to the bridging oxygen rows [16,17].

Fig. 5 shows Fourier transform of the EXAFS oscillation along the $[0\,0\,1]$ direction in the *k*-range of 30–$80\,\mathrm{nm}^{-1}$. A peak appeared at about 0.25 nm, which is more relevant to Mo–Mo in Mo metal than Mo–O bonding. Curve fitting analysis was carried out on inversely Fourier transformed data over 0.2–0.3 nm assuming Mo–Mo bond using EXAFS equation (2).

$$\chi(k) = \frac{SN^* F(k) \sin(2kr + \phi(k)) \exp(-2k^2\sigma^2)}{kr^2} \quad (2)$$

where S, N^*, r, s, $F(k)$ and $\phi(k)$ are overall reduction factor, effective co-ordination number, inter-atomic bond length, Debye–Waller factor, backscattering amplitude and phase shift for Mo–Mo bond, respectively. k is the wave number of photoelectron.

$$k = \sqrt{\frac{2m}{\hbar^2}(h\nu - E_0)} \quad (3)$$

Table 1
Curve fitting result of Mo on TiO_2(1 1 0) along the [0 0 1] direction

Bond direction	N	r (nm)	E_0 (eV)	σ (10^{-5} nm)
[0 0 1]	5.5 ± 0.8	0.272 ± 0.004	-0.8 ± 2.0	3.6 ± 1.0

where m, $h\nu$ and E_0 are mass of electron, photon energy and the origin of photoelectron kinetic energy, respectively.

The backscattering amplitude, $F(k)$ and the phase shift, $\phi(k)$ were calculated by an FEFF code [28]. S is determined from the EXAFS oscillation of Mo foil. The results are summarized in Table 1. The effective coordination number is nearly 5.5 and the bond length is 0.272 nm. The Mo–Mo bond length, 0.272 nm, well corresponds to that of metallic Mo. We tried to determine the local structures for the other directions but oscillations for the [1 $\bar{1}$ 0] and [1 1 0] directions were so weak that we could not obtain reliable structural parameters. Combining the EXAFS data with the XANES results, it is most plausible that one-dimensional metallic Mo chains grew along the [0 0 1] directions, interacting with the substrate oxygen atoms.

When the Mo chain on TiO_2(1 1 0) was heated at 773 K under the presence of 200 Torr O_2, the surface Mo was lost probably because the interaction between the Mo chain and the substrate was so weak that oxidized Mo species was sublimed under these oxidative conditions.

4. Discussion

In our preliminary LEED experiment on the TiO_2(1 1 0) sample similarly treated, we found (1 × 1) LEED patterns. Thus we postulated that the TiO_2(1 1 0) (1 × 1) surface structure should be maintained after the Mo CVD process. As the results of PTRF-EXAFS, we found Mo–Mo bonding along the [0 0 1] direction of TiO_2(1 1 0). The bonding feature of Mo–Mo is metallic judging from the bond length. This conclusion is supported by the XANES spectra. We observed a metal-like feature in the Mo K-edge along the [0 0 1] direction, whereas those for [1 1 0] and [1 $\bar{1}$ 0] were more oxide-like. The effective coordination number of Mo–Mo along [0 0 1] was 5.5, which suggests the presence of rather long Mo chains because the effective coordination numbers for Mo dimer, trimer, tetramer and Mo chain with infinite length can be calculated by using Eq. (1) to be 3, 4, 4.5 and 6, respectively. XANES spectra in the [1 1 0] and [1 $\bar{1}$ 0] directions indicate the presence of Mo–O bonding, though the analysis of EXAFS failed due to the small oscillations. The weak EXAFS oscillations may be due to the disorder in the Mo–O bondings. The PTRF-EXAFS indicated that the Mo–Mo bond length in the [0 0 1] direction was 0.272 nm, which was shorter than the O–O distance in the [0 0 1] direction of the bridging oxygen row (0.296 nm). Accordingly, the Mo–O distances between the Mo overlayer and the TiO_2 substrate might be distributed in a wide range, which made Debye–Waller factors, σ, of Mo–O larger and EXAFS oscillations weaker [29]. We propose a Mo chain structure model along the [0 0 1] direction with Mo–Mo distance of 0.272 nm (metallic-like) interacting with the TiO_2(1 1 0) surface through Mo–O bonding whose distances are randomly distributed. The Mo chain might be located in the channel at the flank of the bridging oxygen row because Mo–O bonds are present in both [1 1 0] and [1 $\bar{1}$ 0] directions.

Table 2 summarizes the reported overlayer structures of metals and metal oxides on TiO_2(1 1 0). These are classified into four groups. First, metal occupies the substituted position of sixfold Ti under the bridging oxygen in TiO_2 substrate (V/TiO_2) [30]. Second, metal adsorbs over the fivefold Ti (Ca, Na, Pt, Pd/TiO_2) [4,31–34]. Xu et al. [4] studied a small amount of Pd overlayer on TiO_2(1 1 0) by STM and found Pd dimer species over the five-fold Ti along the [0 0 1] axis. These two cases are less than 1 ML deposition. When the deposition amount exceeds 1 ML, film or crystalline growth has been observed. For non-reactive (metallic) overlayer, three-dimensional crystalline growth is often observed but crystalline lattice direction is correlated with the substrate structure. (1 1 1)-oriented f.c.c. Cu and Pt particles grow three-dimensionally on TiO_2(1 1 0) with the overlayer [1 $\bar{1}$ 0] orientation parallel to the substrate [0 0 1] direction [9–11,19–21], indicating that the metal–metal bond is aligned along the [0 0 1] direction. Bourgeois et al. [12] reported a Ni zigzag chain with the Ni–Ni bond length at 0.25 nm along [0 0 1] direction. We have recently studied Cu/TiO_2(1 1 0) structure by means of PTRF-EXAFS and found one-dimensional

Table 2
Metals and metal oxides on $TiO_2(1\,1\,0)$

	Preparation	Method	Results	
Pd/TiO_2	Evaporation, <1 ML	STM	Particles, dimer along [0 0 1]	[4]
Ir, Rh/TiO_2	Evaporation	STM	Particle on defect	[7,8]
Pt/TiO_2	Evaporation	STM, PED	Pt adsorbs on top of 5-fold Ti^{4+}	[32,34]
Pt/TiO_2	Evaporation	ARXPS, LEIS, LEED	3D particle growth, [1 $\bar{1}$ 0] of particle aligned to [0 0 1] substrate	[11]
Pt/TiO_2	Evaporation	PED	3D particle growth, [1 $\bar{1}$ 0] of particle aligned to [0 0 1] substrate	[19–21]
Pt/TiO_2	Evaporation	LEIS	3D particle growth, encapsulation of TiO_x after annealing	[18]
Ni/TiO_2	Evaporation, <1 ML	E-EXAFS*1	Ni chain along [0 0 1]	[12]
Ni/TiO_2	Evaporation	ARUPS	Ni along [0 0 1]	[13]
Ni/TiO_2	Evaporation, 1 ML	Theory (DV-Xα)	Atop site of bridging oxygen	[38]
Cu/TiO_2	CVD, <1 ML	TRFXAFS	Cu along [0 0 1]	[35]
Cu/TiO_2	Evaporation, 50 ML	LEED	3D f.c.c. (1 1 1) Cu particles with Cu[1 $\bar{1}$ 0] parallel to the substrate [0 0 1]	[9]
Cu/TiO_2	Evaporation	LEED, APXPS, MEED	3D f.c.c. (1 1 1) Cu particles with Cu[1 $\bar{1}$ 0] parallel to the substrate [0 0 1]	[10]
V/TiO_2	Evaporation, 1 ML	LEED, XPD	Sixfold titanium sites under bridge oxygen atoms	[30]
V/TiO_2	Evaporation	XPD	2D b.c.c. structure with V[0 0 1] parallel to the substrate [0 0 1]	[36]
VO_2/TiO_2	Evaporation and annealing under O_2	XPS, LEED, XPD	Distorted rutile VO_2[1 1 0] epitaxially growth on TiO_2[1 1 0]	[37]
CaO/TiO_2	Segregation of Ca	STM	Ca occupies the position of the fivefold co-ordinated Ti	[33]
Fe, Cr/TiO_2	Evaporation	LEED	2D b.c.c. structure with [0 0 1] parallel to the substrate [0 0 1]	[14]
Na/TiO_2	Evaporization	LEED, STM	Atop site of fivefold Ti	[31,39]
Mo/TiO_2	Impregnation, <1 ML	TPRF-XAFS	Mo dimer perpendicular to [0 0 1]	[16,17]

Cu metallic chain along the [0 0 1] direction [35]. Morphology of overlayer particles is affected by the substrate surface structure. Berko et al. found that Ir and Rh particles are elongated along the [0 0 1] direction of $TiO_2(1\,1\,0)$ substrate when they are formed by "seeding + growing" procedure [7,8]. In the cases of more reactive elements Cr and V, two-dimensional growth of b.c.c. (1 0 0) oriented crystallines is observed with their [0 0 1] direction parallel to the substrate [0 0 1] direction [14,15,36,37]. Namely, approximately two square unit cells of the overlayer correspond to one rectangular TiO_2 unit cell. The metal registration along the substrate oxygen rows is much better than that in the perpendicular direction due to the smaller lattice mismatch. The deposited Cr and V overlayers were also found to be somewhat oxidized. After annealing of the V overlayer in the presence of O_2, distorted rutile VO_2 grew epitaxially [37].

We found Mo–Mo metallic bonds along the [0 0 1] direction. At the same time, Mo–O bonds are in the [1 $\bar{1}$ 0] and [1 1 0] directions. This growth direction is consistent with those of the reported metallic overlayers. On the other hand, when a sample was prepared by the deposition of $[Mo_7O_{24}]^{6-}$ and annealed under oxidative conditions, Mo dimers were formed on $TiO_2(1\,1\,0)$ with the Mo–Mo bond perpendicular to the [0 0 1] direction [16]. We can tentatively postulate that the low valence Mo species having metallic character are arranged along the [0 0 1] direction, while high valence species are bound directly to the bridging oxygen, which may be a driving force to form the dimers perpendicular to the [0 0 1] direction. These

results also provide an example for the possibility to control the structure and orientation of the deposited materials by the preparation process.

5. Conclusion

The Mo species on TiO_2(1 1 0) was prepared by CVD technique under the reduction conditions. Three different PTRF-EXAFS oscillations clarified the Mo–Mo bonding parallel to the [0 0 1] axis of TiO_2(1 1 0) surface. In situ PTRF-EXAFS technique is one of the promising techniques to determine the interface structure and orientation of metal and metal-oxide species supported on single crystal surfaces.

Acknowledgements

This work has been supported by CREST (Core Research for Evolutional Science and Technology) of Japan Science and Technology Corporation (JST) and performed under the approval of the Photon Factory Advisory Committee (Proposal No. 97G063).

References

[1] V.E. Henrich, P.A. Cox, The Surface Science and Metal Oxides, Cambridge University Press, Cambridge, 1994.
[2] H. Onishi, K. Fukui, Y. Iwasawa, Bull. Chem. Soc. Jpn. 68 (1995) 2447.
[3] J. Nerlov, Q. Ge, P.J. Møller, Surf. Sci. 348 (1996) 28.
[4] C. Xu, X. Lai, G.W. Zajac, D.W. Goodman, Phys. Rev. B 56 (1997) 13464.
[5] G. Charlton, P.B. Howes, C.L. Nicklin, P. Steadman, J.S.G. Taylor, C.A. Muryn, S.P. Harte, J. Mercer, R. McGrath, D. Norman, T.S. Turner, G. Thornton, Phys. Rev. Lett. 78 (1997) 495.
[6] B. Hird, R.A. Armstrong, J.A. Seel, Surf. Rev. Lett. 5 (1998) 309.
[7] A. Berko, G. Klivenyi, F. Solymosi, J. Catal. 182 (1999) 511.
[8] A. Berko, I. Ulrych, K.C. Prince, J. Phys. Chem. 102 (1998) 3379.
[9] P.J. Moller, M.C. Wu, Surf. Sci. 224 (1989) 265.
[10] J.M. Pan, B.L. Maschhoff, U. Diebold, T.E. Madey, Surf. Sci. 291 (1993) 381.
[11] H.P. Steinruck, F. Pesty, L. Zhang, T.E. Madey, Phys. Rev. B 51 (1995) 2427.
[12] S. Bourgeois, P. Le Seigneur, M. Perdereau, D. Chandesris, P. Le Fevre, H. Magnan, Thin Solid Films 304 (1997) 267.
[13] H. Onishi, T. Aruga, C. Egawa, Y. Iwasawa, Surf. Sci. 233 (1990) 261.
[14] J.M. Pan, U. Diebold, L. Zhang, T.E. Madey, Surf. Sci. 295 (1993) 411.
[15] J.M. Pan, B.L. Maschhoff, U. Diebold, T.E. Madey, Surf. Sci. 291 (1993) 381.
[16] W.-J. Chun, K. Asakura, Y. Iwasawa, Chem. Phys. Lett. 288 (1998) 868.
[17] W.-J. Chun, K. Asakura, Y. Iwasawa, J. Phys. Chem. 102 (1998) 9006.
[18] F. Pesty, H.P. Steinruck, T.E. Madey, Surf. Sci. 339 (1995) 83.
[19] K. Tamura, M. Owari, Y. Nihei, Bull. Chem. Soc. Jpn. 61 (1988) 1539.
[20] K. Tamura, U. Bardi, Y. Nihei, Surf. Sci. 216 (1989) 209.
[21] K. Tamura, M. Kudo, M. Owari, Y. Nihei, Chem. Lett. (1986) 1921.
[22] M. Shirai, Y. Iwasawa, in: Y. Iwasawa (Eds.), XAFS Application to Catalysis and Surface, World Scientific, Singapore, 1996, p. 332.
[23] K. Asakura, W.-J. Chun, Y. Iwasawa, Topics in Catal., in press.
[24] M. Heald, E. Keller, E.A. Stern, Phys. Lett. 103A (1984) 155.
[25] S.M. Heald, H. Chen, J.M. Tranquada, Phys. Rev. B 38 (1988) 1016.
[26] K. Asakura, in: Y. Iwasawa (Ed.), X-ray Absorption Fine Structure for Catalysts and Surfaces, World Scientific, Singapore, 1996, p. 33.
[27] S. Stizzax, G. Mancini, M. Benfatto, C.R. Natoli, J. Carcia, A. Bianconi, Phys. Rev. B 40 (1989) 12229.
[28] J.J. Rehr, R.C. Albers, S.I. Zabinsky, Phys. Rev. Lett. 69 (1992) 3418.
[29] B.K. Teo, EXAFS: Basic Principles and Data Analysis, Springer, Berlin, 1986.
[30] M. Sambi, E. Pin, G. Sangiovanni, L. Zaratin, G. Granozzi, F. Parmigiani, Surf. Sci. 349 (1996) L169.
[31] H. Onishi, Y. Iwasawa, Catal. Lett. 38 (1996) 89.
[32] K.D. Schierbaum, S. Fischer, M.C. Torquemad, J.L. de Segovia, E. Roman, J.A. Martin Gago, Surf. Sci. 345 (1996) 261.
[33] H. Noerenberg, J.H. Harding, Phys. Rev. B 59 (1999) 9842.
[34] S. Fischer, K.D. Schierbaum, W. Gopel, Vacuum 48 (1997) 601.
[35] K. Asakura, W.J. Chun, Y. Tanizawa, Y. Iwasawa, PF Activity Report B16 (1999) 79.
[36] M. Sambi, E. Pin, G. Sangiovanni, L. Zaratin, G. Granozzi, F. Parmigiani, Surf. Sci. 349 (1996) L169.
[37] M. Sambi, G. Sangiovanni, G. Granozzi, Phys. Rev. B 55 (1997) 7850.
[38] P.L. Cao, D.E. Ellis, V.P. Dravid, J. Mater. Res. 14 (1999) 3684.
[39] H. Onishi, T. Aruga, C. Egawa, Y. Iwasawa, Surf. Sci. 199 (1988) 54.